

## Formation of $H^-$ and $D^-$ ions by hydrogen and deuterium particle backscattering from alkali-metal surfaces

J. R. Hiskes

*Lawrence Livermore National Laboratory, University of California, Livermore, California 94550*

P. J. Schneider\*

*Lawrence Berkeley Laboratory, University of California, Berkeley, California 94720*

(Received 14 July 1980)

A model has been developed for the generation of negative ions by particles backscattered from alkali-metal surfaces. The negative-ion secondary-emission coefficient (NISEC) is taken to be the product of the backscattered particle energy and angular distribution, a negative-ion formation probability, and a survival probability. The backscattered distributions are calculated using the Marlowe Monte Carlo reflection code. The formation and survival probabilities have exponential forms with adjustable parameters  $\alpha$ ,  $\beta$ . A least-squares fit of the NISEC integral to the experimental data provides semiempirical values for the  $\alpha$ ,  $\beta$ . The survival probabilities are found to vary inversely with surface work function. The formation probabilities are dependent upon work function and valence electron density. The semiempirical survival probabilities are in fair agreement with earlier model calculations. The quality of the least-squares fits together with the survival probability comparisons represents a first point of contact for theory and experiment.

### I. INTRODUCTION

The formation of negative hydrogen ions by energetic particles backscattering from crystal surfaces is enhanced by particle reflection from low work function materials.<sup>1,2</sup> Alkali metals and alkali-transition-metal complexes exhibit surface work functions in the range from above 1 eV up to about 3 eV. The reflected fraction of incident particles in turn is increased by selecting metal targets with high atomic number. For incident particle energies below 1 keV, the reflected fractions may exceed 50%. The combination of a partial monolayer of alkali metal absorbed on a high-Z substrate provides for an optimum reflection coefficient together with a low surface work function. These considerations have formed the basis for the development and interpretation of hydrogen negative-ion systems employing active alkali surfaces.

In this paper we continue the development of the surface model for the formation of negative hydrogen ions.<sup>3-7</sup> In its essential form, the negative-ion secondary-emission coefficient (NISEC) is taken to be equal to the product of three factors: the fraction of incident particles backscattered through the surface; the probability of formation of negative ions in the near-surface region; and the survival probability of the negative ions as they recede to great distances away from the surface. The model has been applied to an analysis of backscattering yields from sodium and Na-Cu.<sup>2,5</sup> With the availability of additional

NISEC experimental data appropriate to the other alkali metals,<sup>2,8</sup> it has become possible to extend and to test the formation model over a broader parameter range. We present here a discussion of the NISEC for energetic hydrogen or deuterium incident normally upon Li, Na, K, Rb, Cs, and the composite surface, Na-Cu.

### II. BACKSCATTERING DISTRIBUTIONS

The reflected fractions, energy, and angular distributions of the backscattered particles are calculated using the Marlowe Monte Carlo code developed by Robinson and Torrens,<sup>9</sup> and Oen and Robinson.<sup>10</sup> The code has been made available by the Oak Ridge group for negative-ion studies. A comparison of the reflection data from Marlowe with experimental backscattering data for incident energies above 1 keV is given in several papers.<sup>10,11</sup> In much of the discussion of negative-ion formation presented below, we shall have need for reflection data at incident energies less than 1 keV, for which Marlowe is the principal source. In this paper we shall use the terms reflected fraction and backscattering fraction interchangeably.

In general, for normally incident particles the angular distribution of backscattered particles fits a  $\cos\theta$  distribution, where  $\theta$  is the polar angle measured from the normal. In Fig. 1 is shown a histogram of the angular distribution for 200-eV hydrogen incident

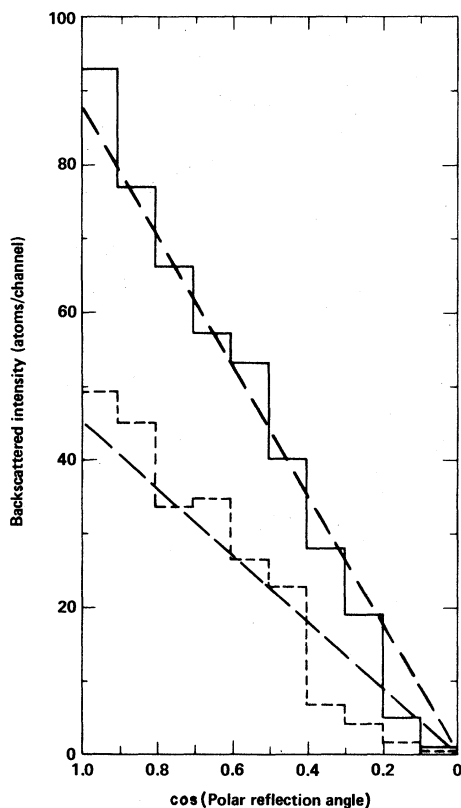


FIG. 1. Histograms of the backscattered intensity of 200-eV incident hydrogen particles plotted vs the cosine of the polar reflection angle. Upper histogram (Cs target); lower histogram (Na target). The dashed diagonal lines would correspond to cosine distributions, respectively.

on Na or Cs, plotted versus the cosine of the polar angle. These data have been obtained from Marlowe for the cases of 4000 and 1000 initial particles upon Na and Cs, respectively. The dashed diagonal lines would correspond to cosine distributions, respectively. For incident energies below 100 eV, deviations from a cosine distribution occur with the reflected distribution tending to peak toward the incident (normal) direction.<sup>10</sup>

In Figs. 2 and 3 are shown histograms of the reflected energy distributions for 200- and 1000-eV hydrogen incident normally upon Na and Cs. The Cs reflected distributions tend to be more peaked toward the incident energy, a consequence of the higher atomic number of cesium and the likelihood for particles to be reflected backward nearer the incident surface. Energy distributions for lithium backscattering are given in Ref. 5.

For purposes of analyzing negative-ion distributions it is more convenient to work with the velocity distribution than with the energy distribution. The backscattered distributions from Marlowe are factored

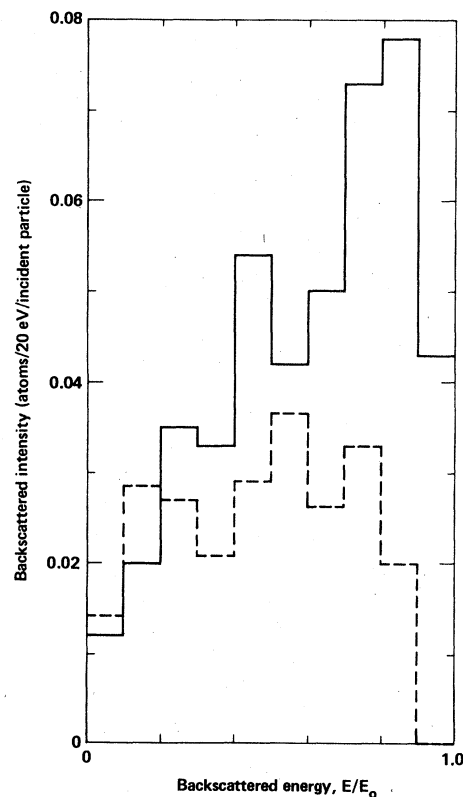


FIG. 2. Histograms of the backscattered intensity of 200-eV incident hydrogen particles plotted vs relative backscattered energy. Dashed histogram (Na target); solid histogram (Cs target).

according to

$$F(v, \theta) dv d(\cos\theta) = 2f(v) \cos\theta dv d(\cos\theta) \quad (1)$$

The fraction of incident particles reflected back through the incident surface is then

$$R_N = \int \int F(v, \theta) dv d(\cos\theta) \quad (2)$$

Reflected fractions for hydrogen incident upon the alkalis with incident energies  $10 \leq E_0 \leq 1000$  eV are given in Ref. 5. In Table I are listed several values of  $R_N$  for both hydrogen and deuterium surface collisions with alkali metals. The  $R_N$  are given in double entry, the upper value pertaining to hydrogen, the deuterium value in parentheses. Inspection of the table shows that for a given alkali target the reflection coefficient falls with increasing incident energy. For a particular value of the incident energy, the reflection coefficient increases with increasing atomic number. To a good approximation the reflection coefficients for the heavier alkalis are functions of incident energy only and independent of the isotopic

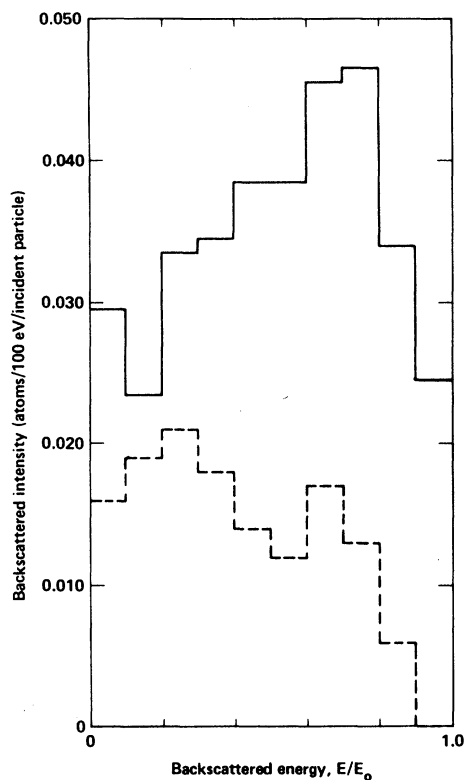


FIG. 3. Histograms of the backscattered intensity of 1000-eV incident hydrogen particles plotted vs relative backscattered energy. Dashed (Na); solid (Cs).

mass of hydrogen versus deuterium. But in the case of lithium the reflection coefficients for hydrogen are substantially larger than for deuterium. This more sensitive isotopic variation for the lighter targets reflects the reduced mass dependence of the two-particle backscattering collision.

The backscattering data displayed here have been obtained using the polycrystalline option available in Marlowe. All the  $R_N$  have been calculated using a minimum of 1000 initial trajectories. For those targets or energies for which the reflection coefficients are low, a larger number of initial trajectories were required in order to obtain relatively smooth histogram distributions. In the case of lithium, as many as 6000 initial trajectories were used. The statistical errors of  $R_N$  are indicated in Fig. 9 of Ref. 5. The  $R_N$  errors for deuterium are less than  $\pm 10\%$ .

### III. NEGATIVE-ION SECONDARY-EMISSION COEFFICIENT

We shall review briefly those features of the formation model necessary for developing the expression for NISEC.

A backscattered particle emerges from the crystal either as a positive ion or an atom. The positive-ion component is presumed to be Auger neutralized in the near surface region and all particles recede from the surface as neutrals. For distances from the surface greater than a few angstroms, the atom gains

TABLE I. Values of  $R_N$  for hydrogen and deuterium collisions with alkali metals.

	150 eV	200	250	300	375	400	500	550	700	1000	1500	2000	3000	4000
Cs		0.44 (0.46)		0.42 (0.45)			0.39 (0.41)		0.38 (0.38)	0.35 (0.40)		0.37 (0.37)		
Rb				0.36 (0.38)	0.36 (0.36)		0.33 (0.32)		0.32 (0.30)	0.30 (0.32)			0.25 (0.25)	
K				0.26 (0.25)	0.23 (0.23)		0.24 (0.22)		0.20	0.20 (0.20)				0.12
Na	0.22	0.23 (0.17)		0.19				0.14 (0.14)	0.16 (0.14)	0.14 (0.13)		0.10 (0.082)		0.047
Li			0.065		0.052		0.045 (0.028)		0.043 (0.025)	0.026 (0.019)		0.016 (0.012)		

and loses an additional electron with rates  $\dot{F}(z)$  and  $\dot{L}(z)$ , respectively, where  $z$  is the particle position measured from the surface. For a particle with specific energy and a velocity component perpendicular to the surface equal to  $v_1$ , the rate of formation of negative ions is given by

$$\frac{dN_-}{dz} = \frac{\dot{F}I}{v_1} - \frac{(\dot{F} + \dot{L})N_-}{v_1} \quad (3)$$

The total particle current, neutral atoms plus negative ions, has been taken equal to the constant  $I = N_0 + N_-$ . Provided the energy level of the active electron is not broadened excessively, the formation and loss regions are distinct and can be localized to  $z_1 \leq z \leq z_2$ , and  $z_2 \leq z \leq z_3$ , respectively. The solution to Eq. (3) becomes

$$N_- = I(1 - e^{-\alpha/v_1})e^{-\beta/v_1} \quad (4)$$

$$K(E_i) = 2 \int \int f_i(v) \cos\theta (1 - e^{-\alpha/v \cos\theta}) e^{-\beta/v \cos\theta} dv d(\cos\theta) \quad (7)$$

This expression can be integrated over  $\cos\theta$  and reduces to an integral over velocity as follows:

$$K(E_i) = 2 \int f_i(v) g(\alpha, \beta, v) dv \quad (8)$$

with  $a = \alpha/v$ ,  $b = \beta/v$ , the  $g(\alpha, \beta, v)$  becomes

$$g(\alpha, \beta, v) = e^{-b}[(1-b)(1-e^{-a}) + ae^{-a}] + 0.57722[(a+b)^2 - b^2] \\ + (a+b)^2 \ln(a+b) - b^2 \ln b + \sum_{n=1}^{\infty} \frac{(-1)^n}{nn!} [(a+b)^{n+2} - b^{n+2}] \quad (9)$$

The velocity distributions,  $f_i(v)$ , are derived from the energy distributions calculated using Marlowe.

Our procedure is to insert experimental  $K(E_i)$  values<sup>2,8</sup> on the left side of Eq. (8) and attempt a least-squares fit of these sets of equations while treating the  $\alpha$  and  $\beta$  as adjustable parameters. Here we employ the iterative fitting procedure in a form developed at LBL (Lawrence Berkeley Laboratory) by Tanis.<sup>14</sup> In analogy with a set of linear equations, we would expect to be able to determine the two parameters  $\alpha, \beta$  by fitting Eqs. (8) to NISEC at two incident energies  $E_{i,j}$ . If we attempt to fit to several data points simultaneously the  $\alpha$  and  $\beta$  are overdetermined. In this latter case one would not be able to obtain a good fit unless the  $f_i(v)$ 's were correct and the functional form of Eq. (7) were essentially correct.

To explore the convergence properties of expression (9), we have experimented with the number of velocity increments,  $\Delta v$ , in the numerical integration [Eqs. (8)], and with the number of terms in the series in Eq. (9). Because of the inverse dependence of  $a$  and  $b$  on velocity, convergence is most difficult at the low-velocity end of the range for the lowest in-

with

$$\alpha = \int_{z_1}^{z_2} \dot{F} dz \quad , \quad \beta = \int_{z_2}^{z_3} \dot{L} dz \quad (5)$$

We shall refer to the second and third factors in Eq. (4) as the formation and survival probabilities, respectively, and to their product,

$$(1 - e^{-\alpha/v_1})e^{-\beta/v_1} \quad (6)$$

as the production probability. If the  $v_1$  varies as the particle moves away from the surface this variation can be incorporated into the  $\dot{F}, \dot{L}$ , and the solution (4) is completely general provided only that  $\dot{F}$  and  $\dot{L}$  do not have overlapping regions in  $z$ . Explicit models for the calculation of  $\beta$  are discussed in Refs. 5, 6, 12, and 13.

The development above is sufficient to write down the expression for NISEC. For particles incident normally with energy  $E_i$ , the NISEC  $K(E_i)$  is taken to be the product of velocity and angle distribution, formation probability and survival probability,

cident energy,  $E_i$ , and for large values of the sum  $(\alpha + \beta)$ . We have found that a minimum of from 50 to 70 terms must be included in the sum, depending on the lowest value of  $E_i$ . NISEC has been evaluated for both five and ten increments in  $v$ , where the backscattered velocity  $v$  ranges from zero to the incident velocity. With sufficient terms for convergence of the sum, the five and ten increment velocity cases give essentially the same values for  $\alpha, \beta$ . We have found that at least three data points,  $E_{i,j,k}$ , must be included in the fitting procedure before the iterative method used here converges smoothly to a final value for  $\alpha, \beta$ . In our routine fits discussed below, we have included 125 terms in the series in expression (9) and ten increments in velocity. The semi-empirical values for  $\alpha, \beta$  found in this procedure are discussed in the next section.

#### IV. EVALUATION OF $\alpha, \beta$ FOR ALKALI METALS

In Figs. 4 and 5 are plotted representative NISEC experimental values for hydrogen and deuterium,

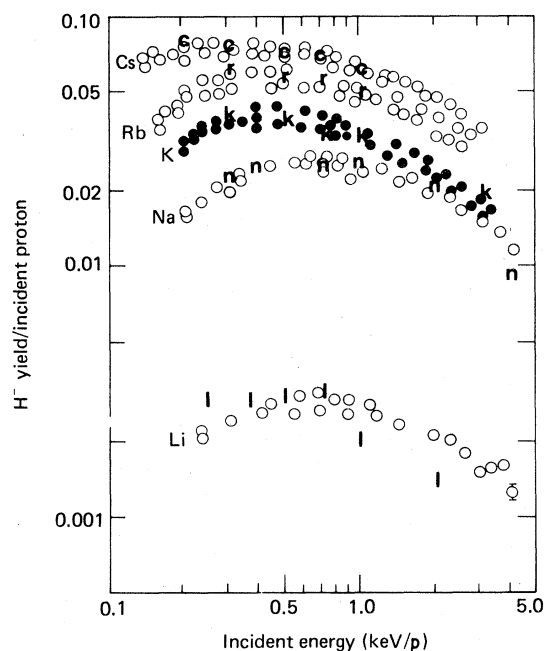


FIG. 4. Experimental NISEC values per proton for hydrogen molecular ions incident normally upon the alkali metals vs the equivalent incident proton energy. Representative data taken from Refs. 2 and 8. The lower case letters are the fits to the data using Eq. (7). The potassium data points are shown as full circles to avoid confusion with the Rb and Na data.

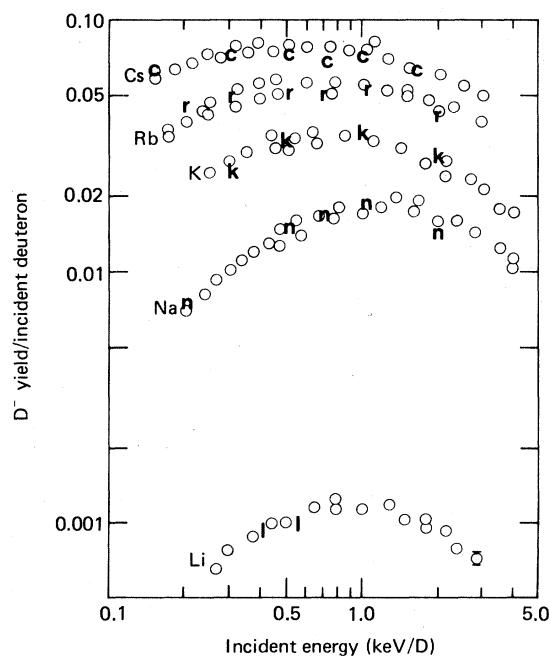


FIG. 5. Experimental NISEC values per deuteron for deuterium molecular ions incident normally upon the alkali metals vs the equivalent incident deuteron energy. The lower-case letters are the fits to the data using Eq. (7).

respectively, incident upon alkali metals. These data are taken from Refs. 2 and 8. Also shown in the figures and indicated by the lower case letters are the fits obtained to Eq. (7). In performing the least-squares fits for a particular alkali, the set of Eqs. (8) are fit simultaneously to both the hydrogen and the deuterium data. The  $\alpha, \beta$  are expected to be functions principally of the surface work function but independent of isotopic mass. This is confirmed by limiting the least-squares procedure to only the hydrogen data, and using the  $\alpha, \beta$  found therein to predict the deuterium NISEC data. For the heavier alkalis the least-squares fits are judged to be satisfactory. In the case of lithium the fitting procedure is not so successful as it is for the other alkalis, although the large difference in NISEC for the hydrogen and deuterium data is reproduced. The NISEC values for lithium are quite small and it is not clear whether the less satisfactory fits here due to experimental uncertainties or a failure in Marlowe to provide accurate velocity distributions.

The semiempirical values for  $\alpha, \beta$  found above are listed in Table II. The  $\alpha, \beta$ 's are normalized such that the velocity of a 200-eV hydrogen atom is equal to unity. The relative errors in the experimental data are quoted as 5%, the systematic errors as 10%. Including these errors in our least-squares-fitting procedure, we judge the  $\alpha, \beta$  to be correct to 10%.

Once having determined the  $\alpha, \beta$ 's one can compute the formation and survival probabilities, the factors given in Eq. (4). These are shown in Fig. 6 and plotted as a function of the perpendicular (normal) energy component,  $E_{\perp}$ , of the reflected particles. The formation probabilities increase toward the lower energies, the survival probabilities increase toward the higher energies.

The formation probabilities decrease in a regular way from Na through Cs, but the Li formation probability lies outside the pattern. This trend from Na through Cs would seem to conflict with one's intuitive feeling that the trend should vary inversely with surface work function (cf. column four in Table II). From its definition in Eq. (5) however, the parameter

TABLE II. Semiempirical values for  $\alpha, \beta$ , the surface work function, and  $\alpha/n_e$  for various targets.

Target	$\alpha$	$\beta$	$\phi$ (eV)	$\alpha/n_e$
Cs	0.39	0.48	1.9	2.1
Rb	0.44	0.58	2.08	1.9
K	0.50	0.65	2.24	1.7
Na	0.94	0.94	2.28	1.7
Li	0.33	0.97	2.42	0.33

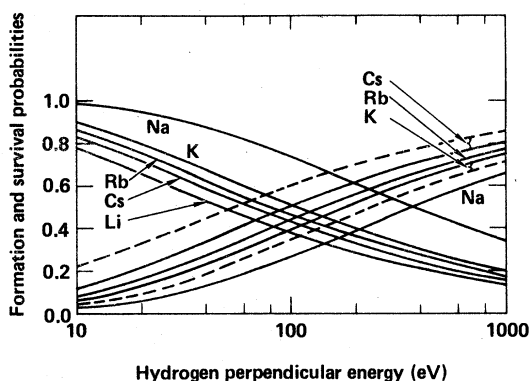


FIG. 6. Formation probabilities (increasing toward the left) and survival probabilities (increasing toward the right) for the alkali metals as deduced from the fitting procedure. The abscissa is the perpendicular component of the backscattered particle energy. The dashed curves represent the theoretical survival probabilities calculated in Ref. 6.

$\alpha$  would be expected to be proportional to the density of occupied electronic states near the Fermi level. In first approximation the density of states is proportional to the density of valence electrons (outermost electron) in the alkali. Dividing the  $\alpha$ 's by the electron density gives the values shown in the last column of Table II. Most of the variation of the  $\alpha$ 's has now been factored out, and the trend is in harmony with the variation of work function. Note the equality of values for K and Na, which have almost identical work functions. We conclude that the formation probability of Na is dominant over that of the heavier alkalis in part due to the higher valence electron density of Na. Li remains anomalous.

Referring again to Fig. 6, we see that the survival probabilities vary in a regular way from Cs through Li (the Li curve is suppressed but would lie immediately below the Na line) and is consistent with the work function trend. Also shown by the dashed lines are the survival probabilities for Cs and K which were calculated previously using a truncated image potential.<sup>6</sup> At 100 eV, the Cs calculations are about 25% high, the K calculations 12% low.

In Fig. 7 are shown the production probabilities, the product of the two functions in Fig. 6. The production probability represents the negative-ion yield that would be obtained if the incident particles were reflected with unit probability together with a relatively narrow energy distribution. The Na probability is dominant over that of the heavier alkalis, due principally to the larger Na formation probability.

#### V. EXTRAPOLATION TO THE Na-Cu COMPLEX

As the adsorbate coverage of the substrate is gradually reduced, the more deeply penetrating particles

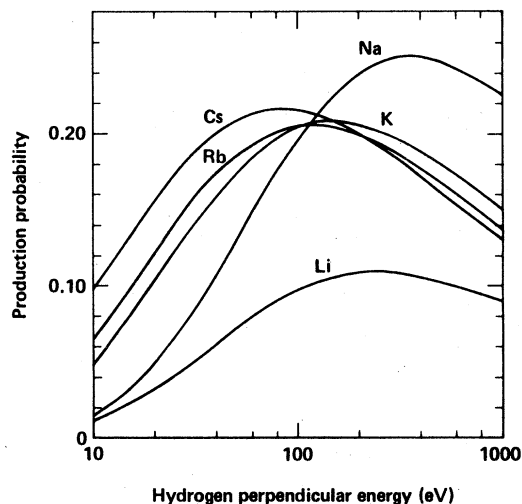


FIG. 7. The production probabilities for the different alkali metals plotted vs the perpendicular component of the hydrogen backscattered energy. For deuterium the energy scale must be doubled.

are increasingly reflected by the substrate material rather than by the adsorbate. For adsorbate coverages only a few layers thick virtually all particles are reflected from the substrate. For these coverages the surface work function and valence electron density are still determined by the adsorbate, however, and retain the bulk adsorbate values.<sup>2,5,8</sup> In the accompanying paper, Ref. 8, it is shown how the NISEC increases by approximately a factor of 2 for the Na-Cu complex as the Na coverage is reduced from the equivalent of bulk Na to a thickness of a few layers, while maintaining the surface work function constant. We shall demonstrate that this increase in NISEC is due to the increased particle reflectivity of copper over that of sodium.

Inserting the  $\alpha$ ,  $\beta$ 's into Eq. (7) found by fitting

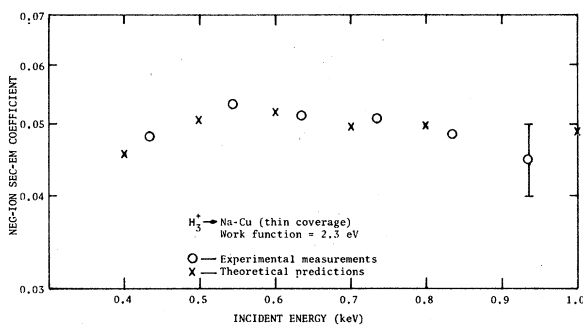


FIG. 8. A comparison of the predicted NISEC's (crosses) using Eq. (7) with the experimental NISEC (circles) for normally incident hydrogen particles onto Na-Cu, plotted vs incident hydrogen energy.

the NISEC data for hydrogen incident on thick sodium (Table II), but replacing the sodium distributions  $f_i(v)$  with the copper distributions computed using Marlowe, Eq. (7) can be used to predict the values for NISEC for the thinner adsorbate coverages. In Fig. 8 these predicted values are compared with the experimental values. Inspection of the figure shows the agreement to be satisfactory and provides further confirmation for the validity of Eq. (7).

## VI. DISCUSSION

We would expect the model<sup>6,7</sup> for negative-ion formation by resonant electron capture from the surface to the outwardly moving atom to break down at higher energies for at least two reasons: the lack of adiabaticity and the weakening of the image potential. The adiabatic potentials derived from the alkali-hydride molecular potentials are suspect for hydrogen energies above a few keV. The classical image potential is weakened due to the finite response time of the surface electrons to a swiftly passing ion.<sup>15</sup> But the expression (7) may have a broader validity than does the resonant electron transfer model, since the expressions (5) are more general. The full range of application of Eq. (7) will not be clear until experimental NISEC data becomes available at higher energies.

We consider next the consequences for our solution (4) upon the assumption that the formation and loss regions are distinct, as expressed by the integration limits in Eq. (5). Extending the range of integrations from  $z_1$  to  $z$  for both  $\alpha$  and  $\beta$  and differentiating Eq. (4) we obtain

$$\frac{dN_-}{dz} = \frac{\dot{F}I}{v_1} - \frac{(\dot{F} + \dot{L})N_-}{v_1} - \frac{\dot{F}I}{v_1} \left[ 1 - \exp \left( -\frac{1}{v_1} \int_{z_1}^z \dot{L} dz \right) \right]. \quad (10)$$

For asymptotically large values of the upper limit  $z$  the last term drops out and Eq. (10) reduces to Eq. (3) provided  $\dot{F}$  is zero at the larger  $z$  values where  $\dot{L}$  is nonzero, and provided  $\dot{L}$  remains zero where  $\dot{F}$  is nonzero. Also, the last term tends to zero as  $v_1$  grows larger. On the other hand if  $\dot{F}$  and  $\dot{L}$  are both nonzero in some range of  $z$ , the last term in Eq. (10) is always negative, and Eq. (10) will integrate to give a smaller value for  $N_-$  than will the correct equation given by Eq. (3). As a consequence our approximate solution [Eq. (4)] will always lie below the exact solution to Eq. (3), but will tend toward the exact solution as  $v_1$  grows larger.

Our procedure here has been to use the solution (4) in Eq. (7), and fit the NISEC to the experimental data in the intermediate energy range above 200 eV. We have used the  $\alpha, \beta$ 's found in this way to extrapolate downward in energy to infer the magnitude of the production probability and NISEC for incident

particle energies as low as 10 eV. From the discussion above it follows that our inferred low-energy values represent lower limits to the correct values for these probabilities.

The formation and production probabilities for Na shown in Figs. 6 and 7 are somewhat larger than reported earlier.<sup>5</sup> Following the preparation of the previous paper, we noticed that for the two lowest velocity increments,  $\Delta v$ , belonging to the NISEC ( $E = 200$  eV) the series in  $g(\alpha, \beta, v)$  was not convergent. The inclusion of additional terms in the series improved the formation probability but the survival probability is essentially unchanged. The fit of the predicted and experimental NISEC's shown in Fig. 8 are also improved. The values shown here supersede those of Ref. 5.

As we have mentioned above, the formation probability for lithium appears anomalous in comparison with those of the other alkalis. Two factors may account for this anomaly. The density of states immediately below the Fermi level in lithium may exhibit a variation substantially less than the mean density of states, a variation that would be in contrast to the other alkalis. Alternatively, the larger work function for lithium may result in the electron transfer to be a nonresonant process while resonant transfer occurs for the heavier alkalis. In analogy with two-body charge transfer in gases, one would expect a considerable reduction in transition rate for the nonresonant process.

## VII. CONCLUSIONS

The quality of the fits of Eq. (7) to the experimental NISEC values, shown in Figs. 4 and 5, together with the predictive fits of Fig. 8, are indicative of a broad range of validity for the theoretical NISEC expression (7). These fits, taken together with the fair agreement of the semiempirical survival probabilities and calculated values, shown in Fig. 6, provide for a first point of contact between theory and experiment in the surface formation of negative ions.

The reflected fractions,  $R_N$ , computed using the Marlowe code have been compared favorably by other workers with experimental reflected fractions for a variety of crystal targets and for incident particle energies above 1 keV. The successful application of the Marlowe energy and angular distributions as they are employed here is suggestive of the validity of Marlowe down to energies as low as 100 to 200 eV.

## ACKNOWLEDGMENT

Work performed under the auspices of the U.S. Department of Energy by the Lawrence Livermore Laboratory under Contract No. W-7405-ENG-48.

- \*Present address: Max Planck Institute for Plasma Physics, Garching, Federal Republic of Germany.
- <sup>1</sup>P. J. Schneider, K. H. Berkner, W. G. Graham, R. V. Pyle, and J. W. Stearns, in BNL Report No. 50727, 1977, edited by K. Prelec, p. 63.
- <sup>2</sup>P. J. Schneider, Ph.D. thesis (University of California, Berkeley, 1980) (unpublished).
- <sup>3</sup>J. R. Hiskes and P. J. Schneider, in 2nd International Conference on Low Energy Ion Beams, Bath, April, 1980 (Institute of Physics Conference Series, in press).
- <sup>4</sup>J. R. Hiskes and P. J. Schneider, *J. Nucl. Mater.* 93, (1980).
- <sup>5</sup>J. R. Hiskes, *J. Phys. (Paris)* 40, C7-179 (1979).
- <sup>6</sup>J. R. Hiskes and A. M. Karo, in BNL Report No. 50727, 1977, edited by K. Prelec, p. 42.
- <sup>7</sup>J. R. Hiskes, A. M. Karo, and M. A. Gardner, *J. Appl. Phys.* 47, 3888 (1976).
- <sup>8</sup>P. J. Schneider, K. H. Berkner, W. G. Graham, R. V. Pyle, and J. W. Stearns, *Phys. Rev. B* 23, 941 (1981) (preceding paper).
- <sup>9</sup>M. T. Robinson and I. M. Torrens, *Phys. Rev. B* 9, 5008 (1974).
- <sup>10</sup>O. S. Oen and M. T. Robinson, *Nucl. Instrum. Methods* 132, 647 (1976).
- <sup>11</sup>W. Eckstein and H. Verbeek, *J. Nucl. Mater.* 76-77, 365 (1978).
- <sup>12</sup>M. E. Kishinevsky, *J. Tech. Phys.* 48, 773 (1978).
- <sup>13</sup>R. K. Janev and S. B. Vojvodic, *J. Phys. B* 13, 2481 (1980).
- <sup>14</sup>J. Tanis (private communication).
- <sup>15</sup>D. L. Mills, *Phys. Rev. B* 15, 763 (1977).